Onset of the aerobic nitrogen cycle during the Great Oxidation Event

Aubrey L. Zerkle[1*], Simon W. Poulton[2], Robert J. Newton[2], Colin Mettam[1], Mark W. Claire[1,3], Andrey Bekker[4], and Christopher K. Junium[5]

[1]*Department of Earth and Environmental Sciences and Centre for Exoplanet Science, University of St Andrews, St Andrews, KY16 9AL, Scotland, UK*

[2]*School of Earth & Environment, University of Leeds, Leeds, LS2 9JT, England, UK*

[3]*Blue Marble Space Institute of Science, P.O. Box 88561, 98145, Seattle, WA, USA*

[4]*Department of Earth Sciences, University of California-Riverside, Riverside, CA, 92521, USA*

[5]*Department of Earth Sciences, Syracuse University, Syracuse, NY, 13244, USA*

resubmitted to *Nature* on 17th November, 2016

*corresponding author az29@st-andrews.ac.uk

The rise of oxygen on early Earth (~2.4 Ga ago)[1] caused a reorganization of marine nutrient cycles[2,3], including that of nitrogen, which is important for controlling global primary productivity. However, current geochemical records lack the temporal resolution to directly address the nature and timing of the biogeochemical response to oxygenation[4]. Here we couple records of ocean redox chemistry with nitrogen isotope ($\delta^{15}N$) values from ~2.31 billion-year-old shales[5] of the Rooihoogte and Timeball Hill formations in South Africa deposited during the early stages of Earth's first rise in atmospheric oxygen[6]. Our data fill a ~400 million-year gap in the temporal $\delta^{15}N$ record[4] and provide evidence for the first pervasive aerobic marine nitrogen cycle. The interpretation of our nitrogen isotope data in the context of Fe speciation and carbon isotope data suggests biogeochemical cycling across a dynamic redox boundary, with primary productivity fuelled by chemoautotrophic production and a nitrogen cycle dominated by nitrogen loss processes utilizing newly available marine oxidants. This chemostratigraphic trend constrains the onset of widespread nitrate availability associated with ocean oxygenation. The rise of marine nitrate could have allowed for the rapid diversification and proliferation of nitrate-utilizing cyanobacteria and, potentially, eukaryotic phytoplankton.

Nitrogen (N) is an essential element for all living organisms, required alongside carbon (C) and phosphorus (P) for the formation of nucleic acids and proteins. As a result, N and P are the principal limiting nutrients controlling autotrophic CO_2 fixation, which in turn regulates climate, weathering, and the redox state of Earth's surface on geologic timescales.

The marine nitrogen cycle is driven largely by biological processes. The primary source of N to the biosphere is nitrogen fixation, the conversion of atmospheric N_2 to organic nitrogen in its bioavailable form (ammonium, NH_4^+). In the modern oceans, ammonium is oxidized via the stepwise process of nitrification, producing nitrite (NO_2^-) and nitrate (NO_3^-). Nitrate (and nitrite) can be assimilated into organic matter, by both oxygenic photoautotrophic bacteria (cyanobacteria) and eukaryotic phytoplankton. Fixed nitrogen is mostly recycled in the water column, but some sinks to the sediments where it is buried and/or remineralized. Some bioavailable nitrogen in the modern oceans is returned to the atmosphere as N_2 via denitrification (the reduction of NO_3^-) and anaerobic ammonium oxidation (anammox, the oxidation of NH_4^+ with NO_2^-) in oxygen-minimum zones[7].

Each of these transformations can affect the ratio of nitrogen isotopes ($\delta^{15}N = (^{15}N/^{14}N)_{sample} / (^{15}N/^{14}N)_{atmospheric\ N2} - 1$, measured in permil, ‰), producing fractionations between reactant and product N species[8]. Nitrogen fixation produces small negative fractionations from atmospheric N_2, resulting in organic $\delta^{15}N$ values of -4 to 0‰[9]. Denitrification and anammox preferentially return the lighter isotope to the atmosphere, leaving the residual nitrate and nitrite enriched in ^{15}N by 10-25‰[8,10]. Large fractionations can also be produced by nitrification and biological assimilation[11] (and possibly by dissimilatory nitrate reduction to ammonium[12]). However, these fractionations are not expressed in most modern environments, since nitrification and the recycling of fixed N compounds occur rapidly and nearly quantitatively. Hence, nitrogen loss via denitrification and anammox dominates the modern nitrogen isotope signal, resulting in sedimentary organic matter with

73 average $\delta^{15}N$ values of 7‰[13], due to the uptake of ^{15}N-enriched residual nitrate by primary
74 producers.

75 Beaumont and Robert[2] were the first to suggest a secular trend in the nitrogen isotope
76 values of organic N for Archean and early Proterozoic sediments. They noted that the $\delta^{15}N$ of
77 kerogen in Archean cherts centered at ~0‰ (ranging from -6 to +13‰), while the $\delta^{15}N$ of
78 early Proterozoic kerogens centered at ~5‰, with a total range similar to that in Phanerozoic
79 sediments (~0 to 10‰) (Fig. 1). Our statistical treatment of the temporal $\delta^{15}N$ record
80 (Extended Data Fig. 1) alongside more recent compilations[14] supports this shift, which occurs
81 broadly coeval with the Great Oxidation Event (GOE) from 2.45-2.32 billion-years-ago
82 (Ga)[1,15], although its precise timing remains poorly constrained. As such, the secular rise in
83 $\delta^{15}N$ is commonly interpreted to reflect the transition from an anaerobic nitrogen cycle
84 dominated by reduced N species (N_2 and NH_4^+), to a modern-style aerobic nitrogen cycle
85 with nitrate as a significant component of dissolved inorganic nitrogen. Small (~2 to 5‰)
86 positive excursions in $\delta^{15}N$ within older (~2.6-2.5 Ga) sedimentary rocks have been
87 interpreted to represent the temporary onsets of nitrification/denitrification during transient or
88 localized oxygenation events, which were apparently not sufficiently widespread or long-
89 lived for the signal to persist[16,17]. Alternatively, these small and short-lived positive shifts in
90 $\delta^{15}N$ recorded exclusively in deep-water facies could reflect the incorporation of ^{15}N-enriched
91 NH_4^+ produced by partial nitrification, assimilation of ^{15}N-depleted NH_4^+ in shallow waters,
92 or nitrogen redox cycling independent of surface oxygenation[4,18,19]. To date, however, no
93 records of contemporaneous shallow-water sediments linked directly to records of ocean or
94 atmospheric oxygenation have been available to test these alternatives.

95 Here we examine the response of the nitrogen cycle to changing atmosphere and
96 ocean redox conditions during deposition of ~2.31 Ga siliciclastic rocks, filling a ~400
97 million-year gap in the temporal $\delta^{15}N$ record (Fig. 1), in sediments contemporaneous with the

98 early stages of the GOE. We focus our analyses on the Rooihoogte and Timeball Hill (R-TH)
99 formations, present in drill core EBA-2 in the Potchefstroom Synclinorium, South Africa
100 (Extended Data Fig. 2 and 3). The R-TH form the basal part of the Pretoria Group in the
101 Transvaal basin, and were deposited on a palaeo-delta slope open to the ocean[1]. U-Pb zircon
102 ages for the tuffs in the lower TH give an age of 2.310 ± 0.009 Ga[5]. Atmospheric oxygen
103 content is constrained by the transition from mass-independent to mass-dependent
104 fractionation of sulfur isotopes recently placed within shales of the Rooihoogte Formation[6]
105 (Fig. 2), indicating a rise in atmospheric O_2 levels to greater than 1 ppm[20]. $\delta^{34}S$ data for
106 sedimentary sulfides in the R-TH also indicate a significant rise in seawater sulfate[1,6],
107 consistent with an increase in oxidative weathering of sulfide minerals on the continents.
108 Additional sample information and discussion of post-depositional alteration is available in
109 the Methods and Extended Data Figures 4 and 5.
110 We used a well-established sequential iron extraction technique[21] (the ratio of highly
111 reactive to total Fe, Fe_{HR}/Fe_T, and the ratio of Fe in pyrite to highly reactive Fe, Fe_{Py}/Fe_{HR}) to
112 assess the redox state of the water column during R-TH deposition. Large variations in iron
113 speciation indicate highly dynamic seawater redox conditions during deposition of the
114 Rooihoogte and the lower ~20 m of the TH formations (Fig. 2), with fluctuations between
115 oxic, ferruginous (anoxic and Fe(II)-rich), and euxinic (anoxic and sulfide-rich) states. The
116 rapid changes in water column chemistry suggest that deposition occurred close to a redox
117 interface (chemocline) between oxygenated surface-waters and anoxic deep-waters that were
118 episodically driven euxinic, possibly by variations in organic carbon delivery or seawater
119 sulfate availability. These data also imply the existence of a transiently sulfidic shelf
120 underlying an oxygenated surface ocean, similar to the redox stratification suggested for the
121 Late Archean[22]. Fluctuations in Fe speciation records are accompanied by a significant
122 increase in total organic carbon (from <1 to ~4%) and a decrease in $\delta^{13}C_{org}$ (from -32 to -

123 36‰) across the R-TH boundary (Fig. 2), consistent with chemoautotrophic carbon fixation
124 at or near a chemocline[23].

125 The $\delta^{15}N$ of both bulk nitrogen, $\delta^{15}N_{bulk}$, and extracted kerogen, $\delta^{15}N_{org}$, show a high
126 degree of variability across this same interval (Fig. 2). When interpreted within the context of
127 the Fe speciation data, these values are consistent with a marine nitrogen cycle developed
128 across a dynamic redox boundary. $\delta^{15}N$ values of 6.0 ± 0.5‰ in the lower part of the section
129 are similar to those of modern marine organic matter[13], which reflect a nitrogen cycle
130 dominated by N loss via denitrification and anammox in oxygen minimum zones[24]. Nitrogen
131 isotope values vary from 1.4 to 12‰ across the R-TH boundary, consistent with a variable
132 input from similar chemotrophic communities across a shifting redox interface. These
133 changes could reflect imbalances in ammonium supply and nitrification-denitrification
134 resulting from periodic upwelling of nutrients and high organic productivity. On a stratified
135 Paleoproterozoic marine shelf, uptake of ammonium from anoxic deep waters would have
136 produced ^{15}N-depleted biomass just below the chemocline. Nitrification with newly available
137 marine oxidants would have further enriched residual ammonium in ^{15}N across the redox
138 interface. Higher $\delta^{15}N$ in oxygenated shallow waters could result from the uptake of this ^{15}N-
139 enriched ammonium, or by nitrate assimilation once nitrate levels rose high enough to
140 support partial denitrification. The $\delta^{15}N$ stabilizes at near modern values (7.2 ± 1.0‰) up-
141 section in the lower TH, in association with Fe speciation data indicative of the onset of
142 pervasively oxygenated shallower water conditions. Oxygenation of surface waters would
143 have supported widespread nitrification and further enhanced nitrate availability.

144 Notably, within the context of the global $\delta^{15}N$ record (Fig. 1), the R-TH succession
145 records the first clear evidence for a long-lived aerobic nitrogen cycle in the sedimentary
146 record. The ~2.31 Ga R-TH section, deposited at the heart of the GOE and coincident with
147 the permanent loss of mass independent S isotope fractionation[6], is bracketed by evidence for

only transient aerobic nitrogen cycling in older sediments (from ~2.7 to 2.5 Ga[16,17,19]), and the clear isotopic imprint of aerobic nitrogen cycling in records from younger sediments deposited after ~2.0 Ga[25-28], as confirmed by statistical analysis of the global database (Extended Data Fig. 1). Available data suggests that earlier transient oxygenation events were insufficient to establish the modern nitrogen cycle, as marine nitrate was not pervasive in the oceans before the GOE[16,17]. In addition, $\delta^{15}N$ values > 2‰ are typical for the remainder of the Precambrian record (Fig. 1), indicating that aerobic nitrogen cycling became at least locally widespread enough to impart a long-lived isotopic imprint on marine $\delta^{15}N$ during the GOE.

The build-up of a significant marine nitrate reservoir would have provided an important evolutionary driver, as prokaryotes and eukaryotic phytoplankton that were able to utilize nitrate as a primary nutrient source could have diversified to fill this new ecological niche. The co-occurrence of this event with other geochemical changes indicative of the first significant oxygenation of Earth's atmosphere provides a crucial constraint on the surprisingly rapid response time of the global biosphere to this major transition in Earth surface chemistry.

References

1 Bekker, A. *et al.* Dating the rise of atmospheric oxygen. *Nature* **427**, 117-120 (2004).

2 Beaumont, V. & Robert, F. Nitrogen isotope ratios of kerogens in Precambrian cherts: a record of the evolution of atmosphere chemistry? *Precambrian Research* **96**, 63-82 (1999).

3 Bekker, A. & Holland, H. D. Oxygen overshoot and recovery during the early Paleoproterozoic. *Earth and Planetary Science Letters* **317-318**, 295-304 (2012).

4 Stueken, E. E., Kipp, M. A., Koehler, M. C. & Buick, R. The evolution of Earth's biogeochemical nitrogen cycle. *Earth-Science Reviews* **160**, 220-239 (2016).

5 Rasmussen, B., Bekker, A. & Fletcher, I. R. Correlations of Paleoproterozoic glaciations based on U-Pb zircon ages for tuff beds in the Transvaal and Huronian Supergroups. *Earth and Planetary Science Letters* **382**, 173-180 (2013).

6 Luo, G. *et al.* Rapid oxygenation of Earth's atmosphere 2.33 billion years ago. *Science Advances* **2**, 1-9 (2016).

7 Dalsgaard, T., Thamdrup, B., Farias, L. & Revsbech, N. P. Anammox and denitrification in the oxygen minimum zone of the eastern South Pacific. *Limnology and Oceanography* **57**, 1331-1346 (2012).

8 Wada, E. in *Isotope Marine Chemistry* (eds E. D. Goldberg, Y. Horibe, & K. Saruhashi) 375-398 (Uchida Rokakuho, 1980).

9 Zerkle, A. L., Junium, C. K., Canfield, D. E. & House, C. H. Production of 15N-depleted biomass during cyanobacterial N2-fixation at high Fe concentrations. *Journal of Geophysical Research* **113** (2008).

10 Brunner, B. *et al.* Nitrogen isotope effects induced by anammox bacteria. *Proceedings of the National Academy of Sciences* **110**, 18994-18999 (2013).

11 Hoch, M. P., Fogel, M. L. & Kirchman, D. L. Isotope fractionation associated with ammonium uptake by a marine bacterium. *Limnology and Oceanography* **37**, 1447-1459 (1992).

12 McCready, R. G. L., Gould, W. D. & Barendregt, R. W. Nitrogen isotope fractionation during the reduction of NO3- to NH4+ by Desulfovibrio sp. *Canadian Journal of Microbiology* **29**, 231-234 (1983).

13 Peters, K. E., Sweeney, R. E. & Kaplan, I. R. Correlation of carbon and nitrogen stable isotope ratios in sedimentary organic matter. *Limnology and Oceanography* **23**, 598-604 (1978).

14 Ader, M. *et al.* Interpretation of the nitrogen isotopic composition of Precambrian sedimentary rocks: Assumptions and perspectives. *Chemical Geology* **429**, 93-110 (2016).

15 Farquhar, J., Zerkle, A. L. & Bekker, A. Geological constraints on the origin of oxygenic photosynthesis. *Photosynthesis Research* **107**, 11-36 (2011).

16 Garvin, J., Buick, R., Anbar, A. D., Arnold, G. L. & Kaufman, A. J. Isotopic evidence for an aerobic nitrogen cycle in the latest Archean. *Science* **323**, 1045-1048 (2009).

17 Godfrey, L. V. & Falkowski, P. G. The cycling and redox state of nitrogen in the Archaean ocean. *Nature Geoscience*, doi:DOI: 10.1038/NGEO633 (2009).

18 Thomazo, C., Ader, M. & Philippot, P. Extreme 15N-enrichments in 2.72-Gyr-old sediments: evidence for a turning point in the nitrogen cycle. *Geobiology* **9**, 107-120 (2011).

19 Busigny, V., Lebeau, O., Ader, M., Krapez, B. & Bekker, A. Nitrogen cycle in the Late Archean ferruginous ocean. *Chemical Geology* **362**, 115-130 (2013).

20 Pavlov, A. A. & Kasting, J. F. Mass-independent fractionation of sulfur isotopes in Archean sediments: Strong evidence for an anoxic Archean atmosphere. *Astrobiology* **2**, 27-41 (2002).

21 Poulton, S. W. & Canfield, D. E. Development of a sequential extraction procedure for iron: implications for iron partitioning in continentally derived particulates. *Chemical Geology* **214**, 209-221 (2005).

22 Reinhard, C. T., Raiswell, R., Scott, C., Anbar, A. D. & Lyons, T. W. A late Archean sulfidic sea stimulated by early oxidative weathering of the continents. *Science* **326**, 713-716 (2009).

23 Coetzee, L. L., Beukes, N. J., Gutzmer, J. & Kakegawa, T. Links of organic carbon cycling and burial to depositional depth gradients and establishment of a snowball

Earth at 2.3Ga. Evidence from the Timeball Hill Formation, Transvaal Supergroup, South Africa. *South African Journal of Geology* **109**, 109-122 (2006).

24 De Pol-Holz, R., Robinson, R. S., Hebbeln, D., Sigman, D. M. & Ulloa, O. Controls on sedimentary nitrogen isotopes along the Chile margin. *Deep-Sea Research Part Ii-Topical Studies in Oceanography* **56**, 1100-1112, doi:10.1016/j.dsr2.2008.09.014 (2009).

25 Godfrey, L. V., Poulton, S. W., Bebout, G. E. & Fralick, P. W. Stability of the nitrogen cycle during development of sulfidic water in the redox-stratified late Paleoproterozoic Ocean. *Geology* **41**, 655-658 (2013).

26 Stueken, E. E. A test of the nitrogen-limitation hypothesis for retarded eukaryote radiation: Nitrogen isotopes across a Mesoproterozoic basinal profile. *Geochimica et Cosmochimica Acta* **120**, 121-139 (2013).

27 Papineau, D. *et al.* High primary productivity and nitrogen cycling after the Paleoproterozoic phosphogenic event in the Aravalli Supergroup, India. *Precambrian Research* **171**, 37-56, doi:10.1016/j.precamres.2009.03.005 (2009).

28 Kump, L. R. *et al.* Isotopic evidence for massive oxidation of organic matter following the Great Oxidation Event. *Science* **334**, 1694-1696 (2011).

29 Farquhar, J., Zerkle, A. L. & Bekker, A. in *Treatise in Geochemistry: Reference Module in Earth Systems and Environmental Sciences* Vol. 6 (eds H. D. Holland & K. Turekian) 91-138 (Elsevier, 2014).

Acknowledgements

This study was supported financially by Natural Environment Research Council Fellowship NE/H016805 to AZ. We thank the Council for Geoscience in South Africa and

the staff at the National Core Library in Donkerhoek for facilitating access to the core materials, and Misuk Yun for assistance with stable isotope analyses at U. Manitoba.

Author contributions

AZ and SP conceived the study; SP and AB collected the samples; AZ, SP, RN, CM, and CJ processed samples and performed geochemical analyses; MC provided statistical analyses of the global database; AZ interpreted the data and wrote the manuscript with input from all coauthors.

Declaration of competing interests

The authors declare no competing financial interests.

Figure Legends

Figure 1. Secular trend in sedimentary $\delta^{15}N$ over early Earth history, from Farquhar et al.[29], with references listed therein. "Mineral N" refers to nitrogen extracted as ammonium from phyllosilicates. Red and purple data points are from this study, denoting kerogen and bulk rock analyses, respectively.

Figure 2. Lithological and geochemical data for core EBA-2, illustrating the R-TH overlying the Great Chert Breccia (GCB), which developed at the top of the Malmani carbonate platform. Data include Fe speciation, TOC, and $\delta^{13}C_{org}$ spanning the section. Fe_{Py}/Fe_{HR} data are only shown for samples with Fe_{HR}/Fe_T suggesting anoxic deposition. Inset is a blow-up of $\delta^{15}N$ values, alongside TOC and $\delta^{13}C_{org}$, for the R-TH boundary (red bar). For $\delta^{15}N$, red data points are extracted kerogen, purple data points are bulk rock N, and empty symbols are

nano-EA analyses. For all data, errors are within the size of the symbols. The orange arrows denote the disappearance of S-MIF in EBA-2[6].

METHODS

Statistical analysis of $\delta^{15}N$ database

Previous studies have utilized age-binned means of the $\delta^{15}N$ database over hand-picked geologic intervals to propose changes in this proxy with time[2,4,14,30]. These studies have provided a qualitative indication that the $\delta^{15}N$ record appears to vary systematically over geologic time; however, they are not statistically robust, because two samples drawn from a single population will often express different means due to random noise. A Student's T-test is a more statistically robust method for determining if two (otherwise normally-distributed) sample sets are likely to arise from the same population, which is considered the null hypothesis. We therefore performed 754 independent two-tailed T-tests spanning every possible time-weighted binning of the $\delta^{15}N$ database, assuming unequal variances in the sample sets. In all but a few cases at the extremes (where the bin sizes of one of the sample sets were small), the null hypothesis was rejected at greater than 99% confidence and so the divided sample sets are shown to arise from populations with different means and variances.

The sample sets are defined as ranging from the first database entry from the Proterozoic, at 0.70 Ga, to the entry with the age shown on the horizontal axis of Extended Data Figure 1, and then from the subsequent entry to our final database entry, with age of 3.80 Ga. Extended Data Figure 1 shows the "false-positive" probability that the two samples sets arise from populations of the same mean and variance. Using this method, datasets at 2.31 Ga (this study), 2.50 Ga, and 2.70-2.80 Ga are demonstrated to be the most statistically meaningful pivot-ages which separate the database into distinct samples sets.

As discussed in the manuscript, the large number of database entries from ~2.50 Ga stem from predominantly deep water environments which show small stratigraphic shifts in $\delta^{15}N$ interpreted to reflect temporary localized nitrification/denitrification in an otherwise reducing ocean[16,17,19]. As a result, the global database may be slightly biased toward results showing an "oxic" nitrogen cycle at this time period. The data presented in this study are from unequivocally oxic shallow waters, and the statistical analysis confirms that our new data provide a stronger statistical power in separating the data sets, even given the bias in the database at 2.50 Ga. As we note in the main text, additional $\delta^{15}N$ data from shallow water depositional environments in this crucial interval are required to test alternative hypotheses.

Although beyond the scope of this current study, we additionally note that the most statistically meaningful separation of the $\delta^{15}N$ database occurs when the sample sets are split between 0.70 – 2.71 Ga and between 2.75– 3.80 Ga. The statistical power for this split is driven primarily by the predominance of extremely ^{15}N-enriched $\delta^{15}N$ measurements (upwards of +55‰, dominantly in kerogens) from this time period. The origin of these extreme values is highly debated, with hypotheses including the onset of partial nitrification[18], and effects from ammonia degassing under highly alkaline conditions[31]. Regardless, it is clear the ~2.70 Ga data do not represent a modern-style aerobic N cycle, as no such extreme values are seen anywhere in the modern Earth system. These statistical analyses therefore demonstrate that the nitrogen cycle underwent massive changes in both the early Neoarchean[31] and at the GOE, with the data from this study forming the key pivot point for the latter.

Fe and C analyses

Iron speciation was determined by means of the sequential extraction technique described in Poulton and Canfield[21], with a RSD of <5% for all extraction steps. TOC was measured on a Leco analyzer after decarbonation by treatment with 20% HCl, with a 1σ of

0.05%. $\delta^{13}C_{org}$ was measured at the SIFIR Laboratory at the University of Manitoba. A calibration line was calculated by least squares linear regression of analyses of two international standards (USGS40, USGS41) performed at the beginning, middle and end of each run. Replicate analyses of international standard USGS Green River shale SGR-1b ($\delta^{13}C_{org}$ = -29.3±0.1‰ VPDB) alongside unknown samples yielded the results of $\delta^{13}C_{org}$ = -29.5±0.2‰ (n=29).

Kerogen-N isotope analyses

Kerogen was extracted following a method modified from McKirdy and Powell[32] in the Geobiology laboratory at the University of St Andrews. Approximately 100-200 mg of bulk rock powders were decarbonated twice with 10% (v/v) HCl overnight at 40˚C in a clean hood, then transferred to Teflon beakers in a dedicated fume cupboard, where 5mL of 10% HCl + 2mL of concentrated HF was added and volatilized at 40˚C. Residues were rinsed 5x with Milli-Q water. Chloroform was added to the residue, shaken, and allowed to settle in separation funnels for ~30 minutes. Heavy minerals that sank to the bottom were first removed, and then floated kerogen was transferred to a Teflon beaker, dried in a clean hood, and stored in an anaerobic chamber until analysis. A subset of samples were also extracted commercially at Global Geolab Ltd, using techniques similar to those above, except that kerogens were separated out by heavy liquid separation with zinc bromide instead of chloroform. Repeat extracts of the same sample (all plotted in Fig. 2) had consistent $\delta^{15}N_{org}$ values between labs, generally within 1‰ (Source Data).

Kerogen N isotope ratios ($\delta^{15}N_{org}$) were measured using a Eurovector 3028HT elemental analyser fitted with a Costech Zero Blank autosampler coupled to an Isoprime isotope ratio mass spectrometer, at the University of Leeds. Columns with reagents were fitted to the EA along with either a high-resolution CN GC column (Elemental Microanalysis E3037), or a NCH column (Elemental Microanalysis E3001), as below. A magnesium

perchlorate-carbosorb trap was used to trap water and CO_2. The setup was leak checked and then the combustion and reduction furnaces were heated to operating temperatures and left purging with He overnight. The combustion furnace was held at 1020°C and the reduction furnace at 650°C. The GC column was baked at 190°C with He flowing overnight, and then its temperature was reduced to the normal running temperature (80°C for the NCH column, and 110°C for the high resolution CN column).

Samples were prepared by weighing between 10 and 30 mg of kerogen into 8 x 5 mm tin cups. These were loaded into the autosampler and purged for at least an hour before analyses. Upon sealing the autosampler chamber and opening it to the main He flow, mass 28 was monitored until it returned to a stable background (less than $7e^{-11}$ nA). Samples were combusted in a pulse of pure oxygen (N5.0 grade, BOC, UK) and injected into a stream of helium (CP grade, BOC, UK). The resulting gases were passed through chromous oxide and silvered cobaltous oxide, fine copper wires, and a magnesium pechlorate/carbosorb trap before entering the GC column. The mass 29/28 ratio of the sample N_2 gas was measured relative to a pulse of pure N_2 (Research grade, BOC, UK) and corrected to the AIR scale using the USGS-25 and USGS-26 ammonium sulfate standards, with $\delta^{15}N_{AIR}$ values of -30.1‰ and +53.7‰, respectively. Repeated runs of standard materials during each analytical session produced standard deviations of the raw $\delta^{15}N_{refgas}$ that were generally between 0.15 and 0.41‰, with the majority ≤ 0.30‰. Data were corrected with bracketing standards using a simple linear regression equation. Repeats of an in-house yeast standard (7.6 wt% N) gave a long-term average value of -0.8 ±0.31‰ (1σ, 37 runs with both NCH and high-resolution CN GC columns), with in-run reproducibility always ≤ 0.2‰ where 3 or more repeats were measured during the same analytical session. A sample size test using the same yeast standard determined that samples producing peak heights of < 1nA have larger variability, approaching the blank $\delta^{15}N$ value as their peak height decreased. Repeat analyses of the yeast

369 standard with peak height > 1 nA produced $\delta^{15}N_{refgas}$ values that differed by ≤ 0.1‰.
370 Therefore, analyses that produced peak heights of < 1nA were discarded in this study.
371 The analysis of organic materials with low concentrations of nitrogen can be
372 complicated by the production of CO gas (at masses 28 and 29) as a result of incomplete
373 combustion, which can alter the apparent $^{15}N/^{14}N$ ratio of the sample. We took the following
374 precautions to ensure that data were not affected by CO production during incomplete
375 combustion: 1) combustion tests using a low-N organic material (cornflower, 0.07 wt% N);
376 2) mass 30 monitoring; and, 3) use of NCH column to produce a better separation between
377 the N_2 and unwanted CO that might produce a secondary mass 28 peak for samples affected
378 by partial combustion.

379 **Bulk-rock analyses**

380 A subset of R-TH samples was analysed for bulk rock geochemistry (wt % K_2O) to
381 screen for post-depositional alteration at the University of St Andrews, using standard X-ray
382 fluorescence (with 1σ of 0.02 wt%). Bulk nitrogen content (% TN) and bulk $\delta^{15}N$ ($\delta^{15}N_{bulk}$,
383 without decarbonation) were measured at the SIFIR Laboratory at the University of
384 Manitoba. Analyses were performed using a Costech^{TM} 4010 Elemental Analyzer (EA) fitted
385 with a Costech Zero Blank autosampler and coupled to a Thermo Finnigan^{TM} Delta V Plus
386 isotope-ratio mass-spectrometer via an open-split interface (ConFlo III, Thermo Finnigan^{TM}).
387 A magnesium perchlorate-carbosorb trap was placed before the ConFlo III to remove
388 remaining water and CO_2. In order to improve the efficiency of sample combustion,
389 temperature in the oxidation column was raised to 1050°C, and a 'macro' O_2 injection loop
390 was utilized. The setup was leak checked and then the oxidation and reduction columns were
391 heated to operating temperatures and left purging with He overnight. The oxidation column
392 was held at 1050°C and the reduction column at 650°C. The ~3 m-long stainless steel GC
393 column was baked at 100-110°C with He flowing overnight, and then its temperature was

reduced to the normal running temperature (55°C). CO_2 level was monitored during analytical sessions. Sample normalization was performed using the two-point calibration described in Coplen *et al.*[33], by analyzing two international standards (USGS40 and USGS41) at the beginning, middle, and end of each analytical session. Two certified standards were additionally analyzed alongside with samples: B2153, soil, % TN = 0.13 ± 0.02%, $\delta^{15}N_{air}$ = +6.70 ± 0.15‰ (Elemental Microanalysis); and SDO-1, Devonian Ohio Shale, % TN = 0.36 ± 0.01%, $\delta^{15}N_{air}$ = -0.8 ± 0.3‰ (USGS). The data obtained were % TN = 0.14 ± 0.00% and $\delta^{15}N_{air}$ values of +6.76 ± 0.02‰ (n=3) for B2153, and % TN = 0.37 ± 0.00% and -0.32 ± 0.02‰ (n=3) for SDO-1.

Nano-EA-IRMS analyses

A subset of extracted kerogens and bulk rock powders were also run for $\delta^{15}N$ by nano-EA-IRMS at Syracuse University, following methods outlined in Polissar *et al.*[34] The benefit of this approach is that it is specifically designed for analysis of as little as 0.5 mg of kerogen and 50 nanomoles of N, thus limiting some of the complications associated with achieving complete combustion on larger samples. Encapsulated sample powders were evacuated to remove atmospheric N_2 present in capsule pore space and purged with Ar. Sample combustion was performed in an Elementar Isotope Cube elemental analyser with reaction conditions set at 1100^{o}C and 650^{o}C for the oxidation and reduction reactors, respectively. Oxygen flow was set a 30 ml*min^{-1} and introduced to the helium stream for 90 seconds, initiating when the sample is dropped into the oxidation reactor. The EA is coupled to an automated cryotrapping system that was build using a modified Elementar TraceGas analyser. The generated N_2 gas was trapped in a silica gel-filled, stainless steel trap cooled in liquid N_2. Following complete collection of the N_2 peak from the high-flow EA, the He flow through the cryotrap was switched to a lower flow (2 ml*min^{-1}) via actuation of a VICI Valco 6-port valve. The trap was heated and N_2 was released to a room temperature capillary GC-

column (JW CarboBOND, 25 m, 0.53 mm ID, 5 µm), and ultimately to the IRMS. The Elementar EA traps CO_2 from combustion in a molecular sieve trap that is released to waste or to the IRMS directly for $\delta^{13}C$ analyses. This ensures that CO_2 is not trapped in the N_2 cryotrap and mitigates the potential for neo-formed CO within the ion source. All samples were run in triplicate and blank-corrected using Keeling-style plots and normalized using the 2pt-correction scheme detailed in Coplen *et al.*[33] Use of Keeling plots allows for simple estimation of the influence of the N_2 procedural blank on samples and for high fidelity measurements of $\delta^{15}N$ on the small sample sizes employed. Reproducibility of replicates analyses of standards [IAEA N1 (0.4‰) and N2 (+20.35‰) and NIST Peach Leaves (1.98‰)] and samples was ± 0.26‰.

Additional analyses and data fidelity

Nitrogen is preserved in the sedimentary rock record primarily as organic N or as ammonium substituting for potassium in phyllosilicates[35]. The sedimentary N isotope values can be modified by a number of post-depositional processes, including diagenesis, burial, and metamorphism. Therefore, before interpreting sedimentary $\delta^{15}N$ data, it is first necessary to examine the possible impacts of post-depositional alteration on the primary signal. Here we examine trends in supplementary and bulk-rock data in order to validate our $\delta^{15}N$ dataset as representing a primary signal.

Degradation of organic matter during early diagenesis can offset primary $\delta^{15}N$ signals by 2 to 3‰[36]. High-pressure metamorphism does not impart significant $\delta^{15}N$ changes [37], although high-temperature metamorphism can increase $\delta^{15}N$ in ammoniated phyllosilicates (and possibly N_{org}; but see Ader *et al.* [38]) due to volatilization of ^{15}N-depleted nitrogen[35,37]. Since the R-TH has only experienced lower greenschist facies metamorphism[23], this mechanism would be expected to produce at most a 1-2‰ positive shift in $\delta^{15}N_{org}$. Cross-plots demonstrate no correlation between % N in kerogen (N_{org}) and $\delta^{15}N_{org}$ values (Extended

444 Data Fig. 4A), rendering no evidence for metamorphic devolatilization of ^{15}N-depleted
445 nitrogen from organics. $\delta^{15}N_{bulk}$ and % total nitrogen (TN) show only a loose positive
446 correlation (with $R^2 = 0.34$; Extended Data Fig. 5A), in the opposite direction of what would
447 be expected from significant loss of ^{15}N-depleted N from whole rocks via devolatilization.
448 Only a weak negative correlation exists between wt % TOC and $\delta^{13}C_{org}$ ($R^2 = 0.42$; Extended
449 Data Fig. 4C), also inconsistent with significant devolatilization of ^{13}C-depleted carbon
450 during metamorphism. These data indicate that loss of N during metamorphism and deep
451 burial did not significantly alter the primary $\delta^{15}N$ (or $\delta^{13}C$) values.

452 Nitrogen isotope exchange can occur between rocks and N-containing compounds
453 when fluids migrate during organic matter maturation[39]. Similar to metamorphism, offset
454 during thermal maturation generally results from preferential volatilization of ^{15}N-depleted
455 nitrogen from organic molecules. The $\delta^{15}N$ of the natural gas is highly variable, but can have
456 $\delta^{15}N$ as low as -12‰[40,41]. Nitrogen isotope exchange during fluid migration would tend to
457 homogenize the isotopic composition of participating N pools, decreasing the isotopic range
458 within the organic N pool and differences between organic and inorganic N pools[39]. Bulk-
459 rock $\delta^{15}N$ ($\delta^{15}N_{bulk}$) covers the measured range of $\delta^{15}N_{org}$, but are generally more positive
460 than $\delta^{15}N_{org}$, inconsistent with complete isotopic homogenization.

461 We observe only a very weak negative correlation between $\delta^{15}N_{bulk}$ and TOC:TN (R^2
462 = 0.29; Extended Data Fig. 5B), suggesting that some ^{15}N-enriched ammonium could have
463 been sorbed onto and/or incorporated into clay minerals in very low-TOC sediments,
464 presumably during exchange with post-depositional fluids. The % TN (but not $\delta^{15}N_{bulk}$)
465 indeed shows a significant positive correlation with % K_2O ($R^2 = 0.81$; Extended Data Fig.
466 5C), supporting incorporation of N into illites during K-metasomatism; however, there is no
467 correlation between $\delta^{15}N_{bulk}$ and % K_2O ($R^2 = 0.10$; Extended Data Fig. 5D), suggesting that
468 this exchange did not significantly affect bulk $\delta^{15}N$ values.

Data Availability Statement

All data generated or analysed during this study are included as source data in this published article.

Extended Data Legends

Extended Data Figure 1. Results from statistical analysis of the $\delta^{15}N$ database, as detailed in the Methods.

Extended Data Figure 2. Stratigraphic context for the Rooihoogte and Timeball Hill formations within the Eastern Transvaal basin, South Africa, and associated ages. "MIF" denotes the disappearance of the mass independent fractionation of sulfur isotopes in the underlying Duitschland Formation (now known to reappear in the Rooihoogte Formation[6]). Modified from Rasmussen *et al.*[5].

Extended Data Figure 3. Simplified geologic map of the Transvaal Supergroup outcrop area (modified from Guo *et al.*[42]), showing the location of drill-core EBA-2. The core is currently stored at the National Core Library at Donkerhoek, which is managed by the Council for Geoscience in South Africa.

Extended Data Figure 4. Cross-plots of kerogen N abundance (% N_{org}) and $\delta^{15}N$ ($\delta^{15}N_{org}$, in ‰), total organic carbon (% TOC) and organic $\delta^{13}C$ ($\delta^{13}C_{org}$, in ‰). For all datapoints, errors are within the size of the symbols.

Extended Data Figure 5. Cross-plots of bulk-rock data, including A. bulk-rock $\delta^{15}N$ ($\delta^{15}N_{bulk}$, in ‰) versus total nitrogen (% TN), B. $\delta^{15}N_{bulk}$ versus TOC:TN atomic ratios, C. % TN versus K_2O content (%), and D. $\delta^{15}N_{bulk}$ versus K_2O content. For all datapoints, errors are within the size of the symbols.

Additional References

30 Thomazo, C. & Papineau, D. Biogeochemical cycling of nitrogen on the early Earth. *Elements* **9**, 345-351 (2013).

31 Stueken, E. E., Buick, R. & Schauer, A. J. Nitrogen isotope evidence for alkaline lakes on late Archean continents. *Earth and Planetary Science Letters* **411**, 1-10 (2015).

32 McKirdy, D. M. & Powell, T. G. Metamorphic alteration of carbon isotopic composition in ancient sedimentary organic matter: New evidence from Australia. *Geology* **2**, 591-595 (1974).

33 Coplen, T. B. *et al.* New guidelines for delta C-13 measurements. *Analytical Chemistry* **78**, 2439-2441, doi:10.1021/ac052027c (2006).

34 Polissar, P. J., Fulton, J. M., Junium, C. K., Turich, C. H. & Freeman, K. H. Measurement of 13C and 15N isotopic composition on nanomolar quantitites of C and N. *Analytical Chemistry* **81**, 755-763 (2009).

35 Boyd, S. R. & Philippot, P. Precambrian ammonium biogeochemistry: a study of the Moine metasediments, Scotland. *Chemical Geology* **144**, 257-268 (1998).

36 Robinson, R. S. *et al.* A review of nitrogen isotopic alteration in marine sediments. *Paleoceanography* **27**, doi:10.1029/2012pa002321 (2012).

37 Bebout, G. E. & Fogel, M. L. Nitrogen-isotope compositions of metasedimentary rocks in the Catalina Schist, California: Implications for metamorphic devolatilization history. *Geochimica et Cosmochimica Acta* **56**, 2839-2849 (1992).

38 Ader, M., Boudou, J.-P., Javoy, M., Goffe, B. & Daniels, E. Isotope study of organic ntrogen of Westphalian anthracites from the Western Middle field of Pennsylvania (U.S.A.) and from the Bramsche Massif (Germany). *Organic Geochemistry* **29**, 315-323 (1998).

39 Schimmelmann, A. & Lis, G. P. Nitrogen isotopic exchange during maturation of organic matter. *Organic Geochemistry* **41**, 63-70, doi:10.1016/j.orggeochem.2009.01.005 (2010).

40 Hoering, T. C. & Moore, H. E. The isotopic compositions of the nitrogen in natural gases and associated crude oils. *Geochimica et Cosmochimica Acta* **13**, 225-232, doi:10.1016/0016-7037(58)90024-3 (1958).

41 Murty, S. V. S. Noble-gases and nitrogen in natural gases from Gujarat, India. *Chemical Geology* **94**, 229-240, doi:10.1016/0168-9622(92)90015-3 (1992).

42 Guo, Q. J. *et al.* Reconstructing Earth's surface oxidation across the Archean-Proterozoic transition. *Geology* **37**, 399-402, doi:10.1130/g25423a.1 (2009).

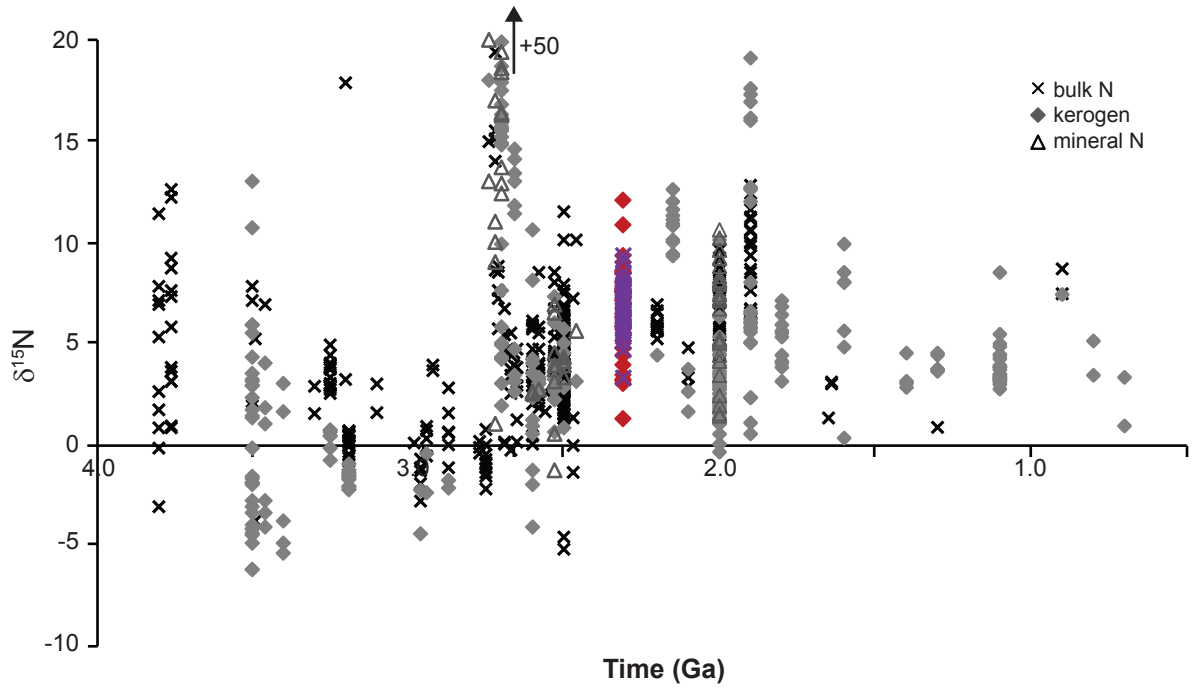
20
15
10
5
0
-5
-10
+50
δ15N
4.0
3.0
2.0
1.0
Time (Ga)
bulk N
kerogen
mineral N

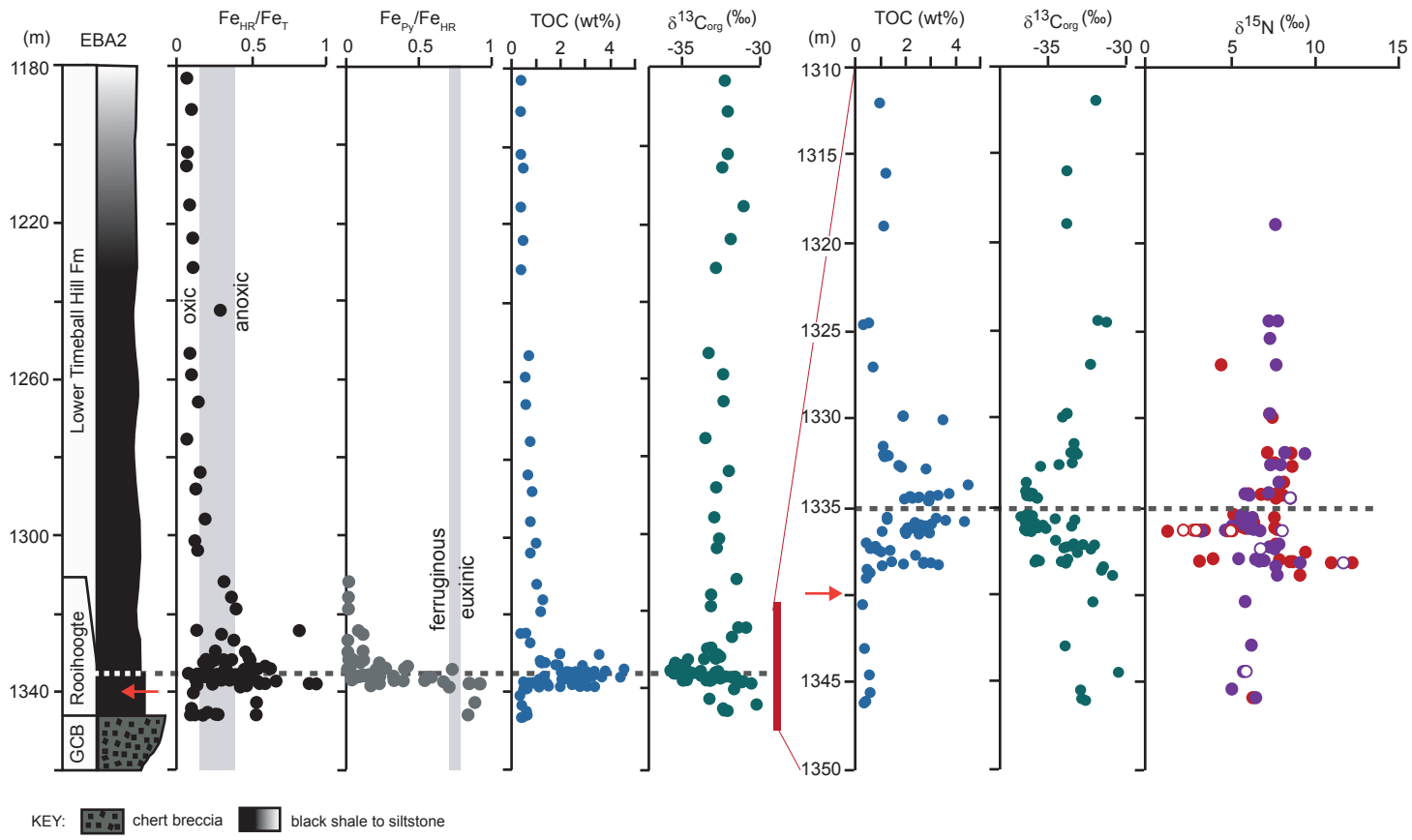
(m)
EBA2
Fe$_{HR}$/Fe$_T$
Fe$_{Py}$/Fe$_{HR}$
TOC (wt%)
$\delta^{13}C_{org}$ (‰)
(m)
TOC (wt%)
$\delta^{13}C_{org}$ (‰)
$\delta^{15}N$ (‰)
1180
1220
1260
1300
1340
1310
1315
1320
1325
1330
1335
1345
1350
0
0.5
1
2
4
-35
-30
5
10
15
Lower Timeball Hill Fm
Rooihoogte
GCB
oxic
anoxic
ferruginous
euxinic
KEY:
chert breccia
black shale to siltstone